Electroabsorption of Lead and Tin-Based Two-Dimensional Perovskites

Introduction
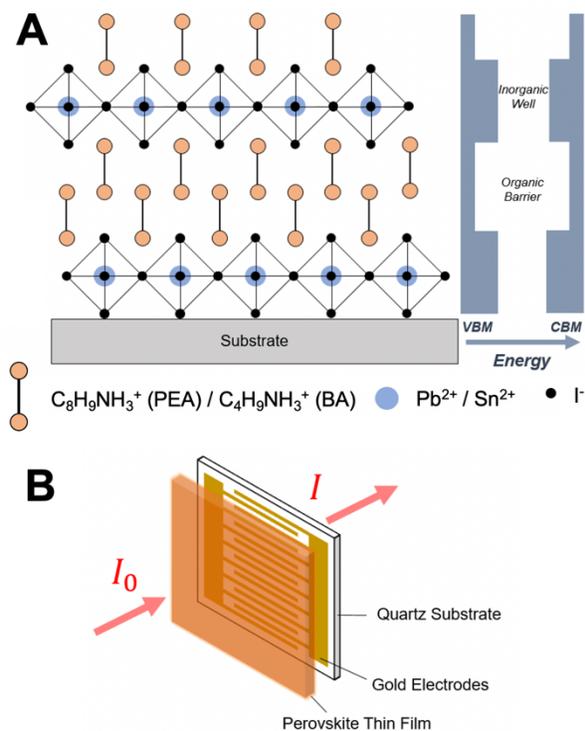
Figure 1. **(A)** 2D MHP multiple quantum well crystal structure consisting of alternating organic-inorganic layers held together by Van der Waals forces. The electronic structure of the semiconducting metal-halide layers dominates the optoelectronic properties at visible wavelengths. **(B)** Schematic of the electroabsorption experiments presented in this report. The interdigitated gold fingers with μm spacing allow for the generation of high electric fields (~10 kV/cm) with modest voltages (~100 V) while also allowing a portion of the incident light to be transmitted for detection.

Two-dimensional metal halide perovskites (2D MHPs) self-assemble to form hybrid organic-inorganic multiple quantum wells (MQWs). The A_2BX_4 crystal structure is shown in **Figure 1A** for the material compositions studied in this report where A = phenethylammonium (PEA^+) or butylammonium (BA^+), B = tin (Sn^{2+}) or lead (Pb^{2+}), and X = iodide (I^-).

2D MHPs were first optically characterized and classified as 2D semiconductors in the early 1990s,[1-3] but did not become the center of significant research efforts until the last five years. The resurgence of interest in these materials has been largely motivated by, one, the impressive rise in photovoltaic performance of 3D MHPs,[4] and two, growing interest in other 2D materials such as graphene, hexagonal boron nitride, and transition metal dichalcogenides.[5, 6] While 2D MHPs application to future optoelectronic devices will undoubtedly grow as a better understanding of their properties is achieved, the materials have already been successfully functionalized as light emitting diodes, photodetectors, electro-optic modulators, polariton lasers, field effect transistors, solar cells, and capping layers for 3D MHP solar cells.[7-11]

One advantage of 2D MHPs is the high level of tunability offered by the range of molecules and atoms which naturally assemble into the A_2BX_4 framework. For example, over 50 different cations have successfully been incorporated into the A-site.[12] Lead, tin, and germanium commonly occupy the B-site metal atom, while the X-site halide atom can vary between iodide, bromide, and chloride. The influence of these compositional degrees of freedom on the 2D MHP electronic structure have yet to be fully explored. Research efforts are naturally allocated to the compositions with highest device performance, and therefore, lead is the most extensively studied B-site metal due to the high photovoltaic performance of the 3D lead MHPs and the intriguing photophysical properties of the 2D PEA_2PbI_4. In this report, we are motivated to test the effects replacing lead with tin on the MHP electronic structure. While it is established that the Sn → Pb substitution both decreases the band gap and increases conductivity, many open questions remain regarding the specific effects of this substitution on the electronic structure.[13-15]

The electronic structure of 2D MHPs can be crudely approximated as that of its single metal-halide BX_4 layer. Since weak Van der Waals forces bind the alternating organic-inorganic layers, the semiconducting BX_4 sheets have negligible electronic coupling to the molecular orbitals in the organic layers. The valence bands are largely comprised of the X-site halide's highest-occupied p orbital anti-bonded to the B-site metal's highest-occupied s orbital. The conduction band, on the other hand, primarily consists of the B-site metal's highest-occupied p orbital. The A-site molecules that comprise the 'barrier

layer' have a comparatively larger band gap energy and lower dielectric constant. Similar to all-inorganic GaAs-based MQWs, the CBM/VBM mismatch between the barrier and well layers creates a quantum confinement effect which increases the electron and hole wavefunction overlap and strengthens the Coulomb attraction. Excitons in 2D MHPs are unique however even in comparison to other MQW systems in that they experience both strong lattice interactions[16, 17] and an image-charge effect from the mismatch in dielectric environments between the organic and inorganic layers.[18, 19] The sum of these effects results in a tightly-bound Wannier exciton with an extremely large exciton binding energy (E_B) on the order of 300 meV.[18, 20, 21]

In this report, we study the band edge properties of both lead and tin-based 2D MHPs using absorbance, photoluminescence, and electroabsorption (EA) spectroscopies. The latter technique is the difference in the material's absorbance with and without an applied external field and is discussed more in **Background Information**. In brief, modulation spectroscopies such as EA have an inherent advantage over traditional spectroscopies due to sharp, derivative-like spectral features at individual critical points in the absorption; these features not only allow for a more precise determination of the critical point's energy, but they also provide additional information on the nature of the states participating in the optical transition. Indeed, EA studies have been critical in advancing the fundamental understanding of the inorganic GaAs-based multiple quantum well (MQW) systems which were the focus of significant research efforts throughout the 1980s.[22, 23] Naturally, researchers first turned to EA in the early 2000s to characterize 2D MHPs. While the technique proved to be critical in demonstrating the anisotropy of the 2D electronic structure, [19, 24, 25] EA spectra on 2D MHPs have yet to be described in great theoretical detail,[26] have led to contradictory interpretations,[20, 21, 25, 27] and exhibit some unexplained spectral features.

In an effort to reconcile these differences and determine which EA features are universal to 2D MHPs, we fabricated EA devices such as that shown in **Figure 1B** with 2D MHP absorbing layers spanning multiple compositions, namely phenethylammonium lead iodide (PEA_2PbI_4), phenethylammonium tin iodide (PEA_2SnI_4), butylammonium lead iodide (BA_2PbI_4), and butylammonium tin iodide (BA_2SnI_4).

The halide I⁻ along with the cations PEA^+ and BA^+ used in this report were chosen to reflect those most commonly incorporated into the 2D MHP framework and used for fabrication of optoelectronic devices. Given the growing relevance of the BA_2SnI_4 and PEA_2SnI_4 materials specifically to devices such as photodetectors, solar cells, and field effect transistors[28-31], more detailed optical and morphological characterization of the materials is correspondingly needed.

Goals and Specific Aims

This work has multiple aims:
1. Use the EA spectra for PEA_2SnI_4 and BA_2SnI_4 to better understand the EA spectral features for all MHPs. Thus far, EA on 3D MHPs has yielded contradictory interpretations and EA on 2D MHPs has only yet been performed for lead-based materials. By expanding the list of MHP compositions for which EA has been reported to include PEA_2SnI_4 and BA_2SnI_4, we hope to gain insight that will elevate our understanding of all previously studied MHP EA spectra.
2. Compare the EA signals of lead and tin-based 2D MHPs (PEA_2SnI_4 vs PEA_2PbI_4) and (BA_2SnI_4 vs BA_2PbI_4) to determine the effect of the Sn→Pb substitution on the electronic structure. More and more, researchers perform this substitution in an effort to make less toxic perovskite devices; however, outside of an increase in conductivity and a decrease in bandgap, there is not much known about the effects of this substitution on the MHP electronic structure. Most importantly, the effect of the Sn→Pb substitution on the value of E_B is unknown.
3. Measure E_B for PEA_2SnI_4 and BA_2SnI_4. The value of E_B will determine the ratio of excitons and free carriers at operation temperatures, and therefore is of critical importance to device engineers. Since E_B is easier to measure for 2D MHPs than their 3D counterparts, E_B of PEA_2PbI_4 and BA_2PbI_4 have been determined with higher confidence and accuracy than any other MHP composition. Thus, measuring E_B for PEA_2SnI_4 and BA_2SnI_4 presents the best opportunity to measure the effect of the Sn→Pb substitution on the value of E_B for all classes of MHPs.

Electroabsorption spectroscopy measures the change in absorbance ΔA in the presence of an applied external field as per the following equation:

$$\Delta A(E) = A(F, E) - A(F = 0, E) \qquad (1)$$

Where F is the applied field and E is the photon energy. Experimentally, the EA signal ΔA is obtained from the normalized electrotransmission $\Delta T/T_0$. Wires are soldered to the vertically oriented gold electrode strips in **Figure 1B** and the EA device is mounted in a cryostat. A broadband light source is passed through a monochromator and focused onto the sample to collect the transmission signal T_0. Next, an AC voltage is applied to the sample and the electrotransmission ΔT is lock-in detected with reference to modulating AC voltage. Since the absorbance is defined as the base 10 logarithm of the transmission spectrum:

$$A(E) = -\log_{10}(T) \qquad (2)$$

the properties of logarithms can be exploited to compute the electroabsorbance (hereafter referred to as electroabsorption) from the normalized electrotransmission:

$$\Delta A(E) = -\log_{10}(T_F) + \log_{10}(T_0) = -\log_{10}\left(\frac{T_F}{T_0}\right) = -\log_{10}\left(\frac{\Delta T + T_0}{T_0}\right) = -\log_{10}\left(1 + \frac{\Delta T}{T_0}\right) \approx -\frac{\Delta T}{T_0}\frac{1}{\ln(10)} \qquad (3)$$

When an electric field is applied to a material, the internal charge densities shift and reorient, hence modifying the nuclear configuration and electronic structure. The electroabsorption spectrum is the difference between the absorption spectrum of the field-perturbed and the unperturbed material states. Since this is a difficult problem outside the scope of analytical solutions, EA spectra are often analyzed using two broad categories of approximations based on what type of charge state is being modulated: bound or unbound states.

Bound states:

For tightly bound states such as molecular orbitals or confined excitons, the change in energy (ΔE) caused by the applied electric field is often largely determined by the relative change in the transition dipole moment (μ_{ge}) and polarizability (α_{ge}) for an optical transition from the ground state (g) to an excited state (e). Modulation of a tightly bound excitonic state can result in a linear or quadratic stark shift proportional to μ_{ge} and α_{ge}, respectively, as described by Stark theory:[32, 33]

$$\Delta E = -\mu_{ge}F - \frac{1}{2}\alpha_{ge}F^2 \qquad (4)$$

where F is the applied electric field. The change in μ_{ge} can be described as the amount of charge-transfer associated with an optical transition, whereas α_{ge} represents the transition's sensitivity to an applied field. Assuming the states are tightly bound, the applied field can be treated as a small perturbation and the EA signal (ΔA) can be approximated by a power-series expansion around a small change in ΔE:[33]

$$\Delta A = -\frac{\partial A}{\partial E}\mu_{ge}F - \frac{1}{2}\frac{\partial A}{\partial E}\alpha_{ge}F^2 + \frac{1}{2}\frac{\partial^2 A}{\partial E^2}(\mu_{ge}F)^2 \qquad (5)$$

In an isotropic solid, the transition dipole moments are randomly oriented and therefore the first term, which is dependent on the field direction $\vec{F}$, averages to zero.
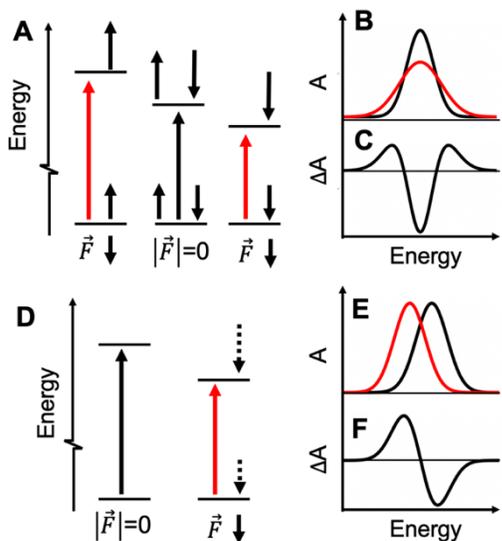
Figure 2. (A) Interaction of an applied electric field with a system of randomly oriented transition dipole moments **(B)** Corresponding broadening and **(C)** resulting change in absorbance. **(D)** Interaction of an applied electric field on a transition with a nonzero change in polarizability between ground and excited states. **(E)** Stark-shifted absorbance peak. **(F)** Resulting EA spectrum due to change in polarizability.

Equation (5), on its own, is a powerful method for analyzing EA spectrum of tightly bound states, such as the 1s exciton state in MHPs. Notice that from this equation we expect the observed EA spectrum to resemble derivative line shapes of the absorption spectrum. Through simple line shape comparison, a large first derivative response can immediately be interpreted as a quadratic Stark effect, typical for Wannier-Mott excitons, whereas a large second derivative response can be interpreted as a linear Stark effect, typical for charge-transfer excitons.

Figure 2 provides a graphical representation of equation (5) that provides strong physical intuition for the derivative-like EA line shapes. Although this is drawn for a molecular system, the principles apply to any bound electronic state. The short/long bolded arrows in **Figure 2A** represent the molecule's permeant dipole moment μ in the ground/excited state, and the difference between the two is defined as μ_{ge}. Notice that a nonzero μ_{ge} gives rise to absorption at lower/higher energies through the linear Stark effect, depending on whether the molecular dipole is parallel/antiparallel to the applied field $\vec{F}$; an ensemble of randomly distributed transition dipole moments will therefore broaden the absorption (**Figure 2B**) and the difference spectrum (EA) has a second-derivative line shape (**Figure 2C**). Examples of absorption features with large μ_{ge} are molecular states with permanent dipole moments[34], charge-transfer excitons[33], and excitons whose charge density has a dipole moment due to morphological disorder.[35]

In **Figure 2D**, the short/long dotted arrows represent the molecule's polarizability in the ground/excited state. Unlike randomly oriented dipoles whose direction of polarization is independent of the applied field, the polarization of charge density due to a state's polarizability will always be parallel with the applied field. Therefore, rather than broadening the absorption, the difference in polarizability between the two states, α_{ge}, uniformly shifts the absorption through the quadratic Stark effect (**Figure 2E**) and the EA resembles a first derivative of the unperturbed absorption (**Figure 2F**). Examples of systems that experience a quadratic Stark effect are polarizable molecules and Wannier excitons. A Stark shift of the latter is formally analogous to a hydrogen atom and is one of the few systems for which EA spectrum has been solved theoretically.[36]

The theoretical EA response of a Wannier exciton includes another phenomenon worthy of mention that is not accounted by equation (5), that is field ionization. When an applied field ionizes a bound state, its lifetime decreases, and its spectra correspondingly broadens according to the time-energy uncertainty principle. Fortunately, a second-derivative line shape due to field-ionization can usually be distinguished from one caused by a large μ_{ge} with careful consideration of the absorption band in question. First, broadening due to field ionization of a bound state below a continuum (such as an exciton) will be asymmetric, as the state will favor ionization into the conduction band.[37] Second, the likelihood of observing field ionization can be readily determined by comparing the applied field strength to the binding energy of the state in question. In the case of an exciton, this is most aptly done by calculating the ionization field, or the field required to create a potential drop of 1 E_B across the exciton's radius (a_B):

$$F_I = E_B/|e|a_B \qquad (6)$$

The value of F_I is on the order of $\sim 10^6$ V/m for 3D MHPs[38] but is on the order $\sim 10^8$ V/m in 2D MHPs, due to the higher E_B in the latter. Since experimental fields are typically on the order of 10^6 V/m, a contribution of spectral broadening due to field ionization is expected in 3D MHPs, but not for 2D MHPs.

Lastly, when considering 2D MHPs, there is another relevant effect that must be considered when the field is applied in the direction of quantum confinement, namely, the quantum-confined Stark effect (QCSE). Similar to the quadratic stark effect, the shift in energy due to the QCSE is negative and scales with the field strength squared. As a result, the exciton resonance redshifts and the EA line shape has a first derivative shape that scales quadratically with field strength.

When applied field are parallel to the 2D MHP quantum wells, however, the QCSE is not relevant. **Figure 3** shows a cartoon representation of expected EA signal for fields parallel to the quantum wells in 2D MHPs, i.e. the geometry employed in the this report. The 1s exciton resonance is expected to redshift due to the quadratic Stark effect. Band-to-band transitions on the other hand result in oscillations in the EA signal. To understand the physical origin of these oscillations, however, a fundamentally different approach is needed since the continuum states are not bounded and electrons are free to accelerate along field lines.

Figure 3. (A) Cartoon representation of the effect an applied field has on a semiconductor's absorbance spectrum. Bound states such as Wannier excitons typically exhibit a quadratic Stark effect whereas free electron states produce FK oscillations. The magnitude of the field-induced shifts are exaggerated since ΔA is typicall on the order of 10^{-4}. **(B)** Corresponding difference signal ΔA, i.e. electroabsorption.

Unbound states:

For unbound states above the band edge, the EA signal response in MHPs is typically described by the Franz-Keldysh (FK) effect.[21, 38] The additional term to the free electron's Hamiltonian (eFz) results in Airy eigenstates, $Ai(x)$ whose argument is the free electron's kinetic energy normalized by an electro-optical energy $\hbar\theta$.[39] The parameters x and $\hbar\theta$ are defined as follows:

$$x = (E - E_g)/\hbar\theta \qquad (7) \qquad\qquad h\theta = (\hbar^2 e^2 F^2/2\mu)^{1/3} \qquad (8)$$

where E is the photon energy, E_g is the band gap, μ is the electron-hole's reduced effective mass and F is the field strength. The difference between exciting into a Bloch vs Airy eigenstates results in oscillations in the EA signal across a spectral range that is proportional to coherence length of free electron states,[40] such as those portrayed on the high energy side of **Figure 3B**. Such oscillations are pronounced for inorganic MQWs[41] but are far more subtle in 2D MHPs.[20, 21] When present, the FK oscillations are discernable from Stark-shifted exciton states not only by their position above the band edge, but also by their field-dependent behavior— FK peak positions broaden inverse the argument of the Airy function $1/x \propto F^{2/3}$ and amplitudes increase proportional to $F^{1/3}$.[39, 42]

When the applied field strength is low and the material exhibits large homogenous broadening (Γ), however, different dependencies of the FK effect are expected. Aspens and Rowe theoretically demonstrated in the 1970s that under a 'low-field' regime when $\hbar\theta < \frac{1}{3}\Gamma$, the EA signal simplifies to a $\chi^{(3)}$ response (similar to the linear and quadratic Stark effects) as is evidenced by the EA signal's field-invariant line shape and quadratic amplitude scaling.[38, 43] However, unlike the linear and quadratic Stark effects, low-field FK EA features cannot be readily identified by comparison of the EA signal to a numerical

4

derivative of the absorbance. In Aspens' theory, field-induced changes in the in the complex dielectric function $\Delta\epsilon(E) = \Delta\epsilon_r(E) + i\Delta\epsilon_i(E)$, (where $\epsilon_r(E)$ represents polarization and $\epsilon_i(E)$ represents the material's absorption) are proportional to the third derivative of the unperturbed complex dielectric constant via the following relationship:

$$\Delta\epsilon(E) = \frac{\hbar\theta^3}{3} \frac{1}{E^2} \frac{d^3}{dE^3} (E^2\epsilon(E)) \tag{9}$$

Thus, agreement in the line shapes of $\Delta\epsilon(E)$ and $\frac{d^3}{dE^3}(E^2\epsilon(E))$ can be taken as evidence of the low-field FK effect. To obtain such a comparison is nontrivial since independent ellipsometry measurements must be performed in conjunction with transfer matrix modeling to relate the EA signal's $\Delta T/T$ to the complex dielectric function $\Delta\epsilon$.[38, 44] Still, provided the band gap is known, low-field FK features can be identified as $\chi^{(3)}$ response above the band edge, i.e. EA features which exhibit field-invariant line shapes and peak amplitude scaling proportional to F^2.

Preliminary Results and Discussion
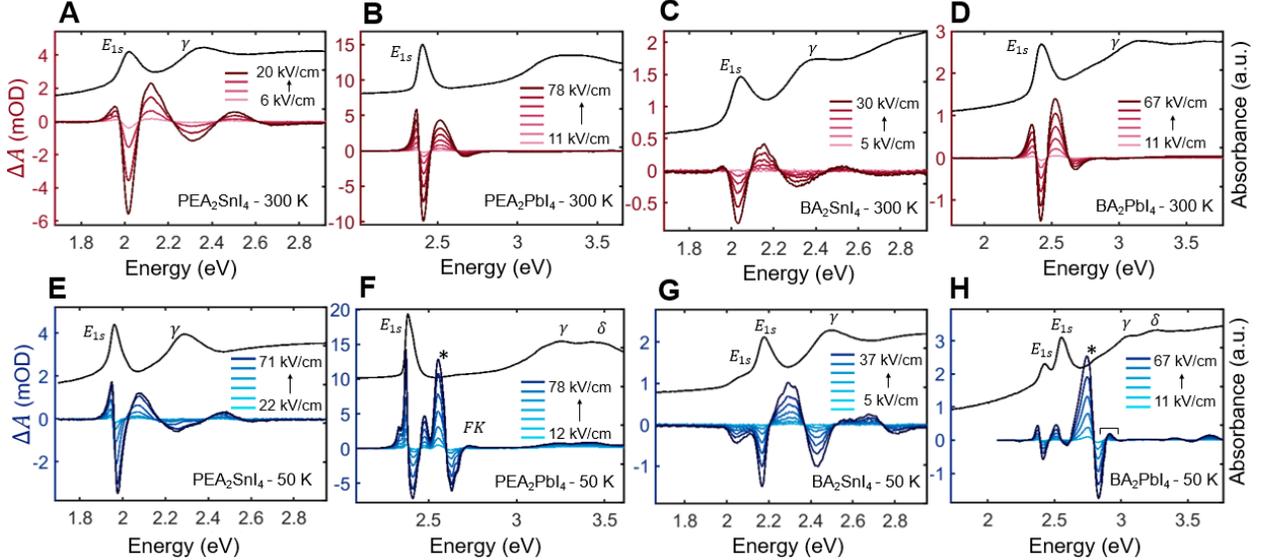
Figure 4. Electroabsorption of 2D MHPs. The 300 K EA spectrum are shown as **(A)** PEA$_2$SnI$_4$ **(B)** PEA$_2$PbI$_4$ **(C)** BA$_2$SnI$_4$ **(D)** BA$_2$PbI$_4$. The 50 K EA spectrum are shown in the same order for panels **(E) - (H)**. The exciton resonance below the band edge (E_{1s}) exhibits both linear and quadratic Stark shifts. Across the band edge, the EA spectral features for the lead-based 2D MHPs show field-dependent broadening indicative of the FK effect. Field broadening is also observed in PEA$_2$SnI$_4$ but much closer to the exciton resonance. The above-gap absorption peaks γ and δ, which are common in all 2D MHP, exhibit EA responses (likely Stark shifts) which supports their hypothesized origin as an overlap of between a secondary CBM and the exciton's continuum of states above the band edge.

EA devices were fabricated by spin casting solutions of dissolved 2D MHP crystals onto thin interdigitated gold electrode strips (**Figure 1B**). In brief, thin films were cast onto an array of thin gold electrodes with small spacing $d = 45$ μm, such that modest voltages could generate high electric fields in-plane with the quantum wells. The transmission T and electro-modulated transmission ΔT were collected and used to calculate the EA signal, $\Delta A \approx -1/\ln(10) \times \Delta T/T$. The comprehensive results for all four 2D MHP compositions are displayed in **Figure 4**. The EA spectra for lead-based 2D MHPs are in excellent agreement with previous studies.[20, 21] EA on tin-based 2D MHPs has not been reported and presents two additional challenges in that one, the Sn$^{2+} \rightarrow$ Sn^{4+} oxidation is rapid and two, the materials are less ohmic.

5

For BA_2SnI_4, an SnF_2 additive was needed to suppress oxidation and increase resistivity. Therefore, PEA_2SnI_4 and PEA_2PbI_4 results present the best direct comparison of tin vs lead with all other experimental parameters held constant. We find that the spectral features of the exciton and continuum are energetically separated for lead-based 2D MHPs but overlap for PEA_2SnI_4, signifying that E_B in tin based MHPs may be far lower than expected. We divide our analysis into two sections, namely, the 1s exciton and the continuum states.

1s Exciton EA response
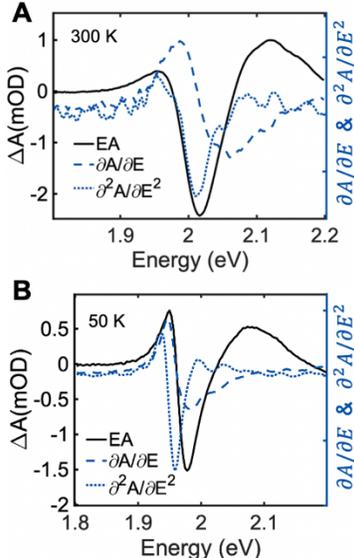
Figure 5. Exciton's EA response for PEA_2SnI_4. **(A)** At 300 K, the EA follows the 2nd derivative of the absorbance whereas at **(B)** 50 K, the EA follows the 1st derivative of the absorbance.

Below the band edge, the EA spectra for all 2D MHPs is dominated by a large Stark shift of the 1s exciton state (marked E_{1s} on the absorbance spectra in **Figure 4**). Although excitons in 2D MHPs are Wannier-like parallel to the quantum wells, the large E_B in 2D MHPs reduce field-ionization effects and therefore the exciton's EA response resembles that of molecular systems rather than inorganic MQWs.[26, 32] These Stark shifts manifest as 1st and 2nd-derivative-like features in the EA signal. Consistent with this analysis, we find the 2D MHP exciton's EA response scales quadratically with field strength and is well fit by a linear combination of numerical 1st and 2nd derivatives of the absorbance spectrum. It was recently discovered that excitons in 2D MHPs have transition dipole moments twice as large as inorganic MQWs ($\mu_{ge} \sim 11$ D for PEA_2PbI_4[45] whereas $\mu_{ge} \sim 6$ D in GaAs-based MQWs[46, 47]). Therefore, as a consequence of equation (5), the linear Stark effect is more relevant to the exciton's EA response in 2D MHPs. Indeed, we find at room temperature that the EA signal follows a 2nd derivative line shape consistent with a large linear Stark effect (**Figure 5A**). Somewhat surprisingly, however, we find the exciton's EA signal transitions to a 1st-derivative line shape at low temperatures (**Figure 5B**). This 2nd to 1st derivative line shape transition moving from 300 K to 50 K is observed in all of the four 2D MHP compositions and has not been reported until now.

A temperature-dependent linear Stark effect has previously only been observed in solvated polar molecules.[48-50] At high temperatures, molecules rotate to align their permanent dipole moments along field lines, whereas at low temperatures the solvent becomes rigid, the molecular rotation is suppressed, and the linear Stark effect diminishes. In 2D MHPs, however, the situation is far different in that excitons do not have permanent dipole moments. The observed temperature dependence here is likely caused by exciton-phonon interactions that diminish concomitant with the depopulation of phonon modes. Morphological disorder has been shown to induce dipole moments of excitons in conductive polymer thin films.[35] We hypothesize the effect here is similar but due to dynamic disorder rather than static morphological disorder. The prior refers to the fluctuating energy landscape caused by the thermal motion in the lattice and is known to play a significant role in excited state dynamics for both 3D and 2D MHP systems.[51, 52] A detailed investigation into the physical origin is beyond the scope of this study, but should be explored theoretically and experimentally with temperature dependent EA and temperature dependent optical Stark effect measurements. We note that the trend is observed for all tested 2D MHPs. In general, there is little variance between the excitonic response of lead and tin-based 2D MHPs.

Continuum EA response

The EA signals for lead and tin-based 2D MHPs diverge much more significantly at higher energies near the band edge. The optical band gap is 2.57 eV for multiple layers of PEA_2PbI_4 and 2.77 eV for BA_2PbI_4 at cryogenic temperatures.[53] Precisely at these energies, a large oscillatory feature appears (marked '*' in **Figure 4**) in the EA signal of lead 2D MHPs at 50 K. We note similar signals have been resolved in conductive polymer films near the band edge for fields parallel to the polymer chain.[54, 55] The field

6

dependence of the * feature differs from the Stark-shifted exciton states— peaks broaden with increasing field and exhibit subquadratic amplitude scaling, as summarized in **Figure 6 A-C** for PEA_2PbI_4. Such field-dependencies are also observed in the tin-based PEA_2SnI_4, but much closer to E_{1s} (Figure 6D).

We attribute this deviation in the EA signal's field dependence to the high-field FK effect. **Figure 6B and 6E** show the peak and zero-crossing positions (marked A-E) broaden with increasing field strength. The average power relation for field-broadening between features, k, (defined as $\Delta XY = AF^k$ where X, Y = A, B, C, D, or E), was found to be $k_{avg} = 0.11$ for PEA_2PbI_4. In comparison, the exciton features show zero field-broadening within the measurement resolution. An identical feature appears in the EA spectrum for BA_2PbI_4 with stronger field broadening, $k_{avg} = 0.20$. The field broadening was strongest however in the tin-based PEA_2SnI_4 ($k_{avg} = 0.39$) (**Figure 6E**). These dependences are all less than the expected $k = 0.66$ for high-field FK oscillations, suggesting the high-field limit is only approached for 2D MHPs.
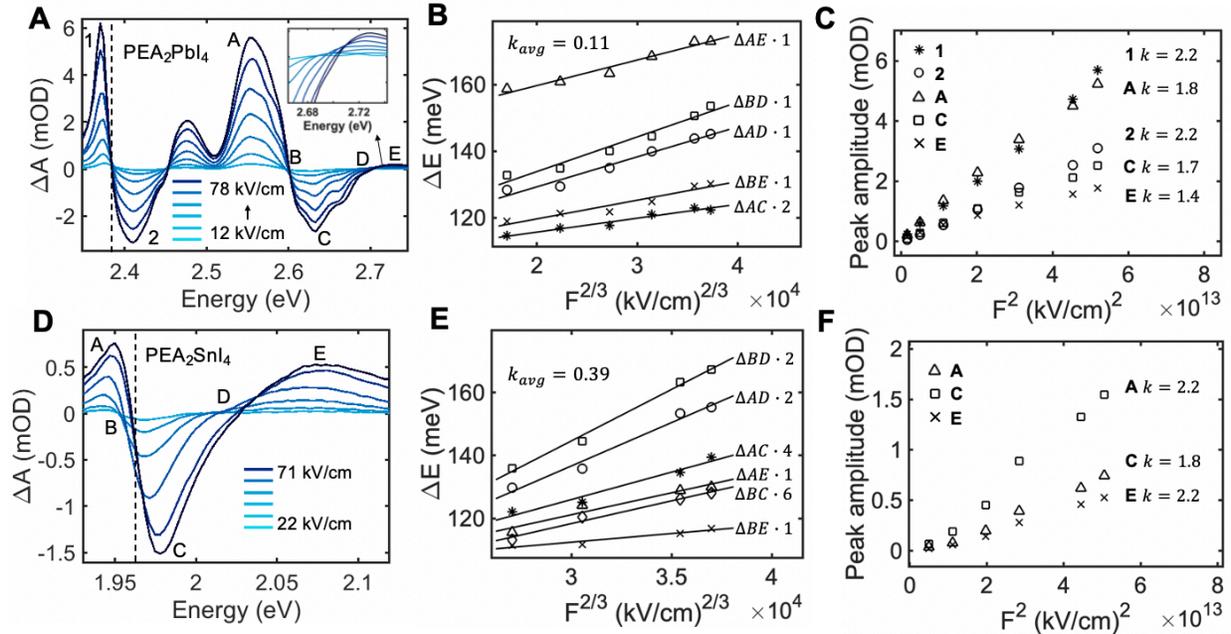
Figure 6. Comparison of FK features for PEA_2PbI_4 and PEA_2SnI_4. **(A)** EA spectrum for PEA_2PbI_4. The dotted line marks the exciton resonance in the absorbance spectrum. Peaks 1 and 2 are assigned to the exciton's quadratic Stark shift whereas A-E are near-gap features with high-field FK character. Inset: expanded view of the FK feature near the band edge. **(B)** Field-broadening as a function of $F^{2/3}$ for PEA_2PbI_4, trends are multiplied for visual comparison of the relative slopes. The average power law scaling between broadened features and field strength ($\Delta XY = F^k$) is $k_{avg} = 0.11$. Low-field data points have been omitted since peak positions are difficult to resolve accurately. **(C)** Peak amplitudes scaling quadratically with field for PEA_2PbI_4. The exciton peak amplitudes '1' and '2' scale with k > 2, whereas the peaks A, C, and E, scale subquadratically (k < 2) with k decreasing as the peaks acquire more high-field FK character at higher energies. The trend for peak E has been multiplied by 10 for easy visual comparison. **(D)** EA spectrum for PEA_2SnI_4 where the dotted line marks the exciton resonance. FK induced field-broadening is observed much closer to exciton resonance, suggesting that tin-based 2D MHPs have a significantly lower binding energies. **(E)** Field-broadening as a function of $F^{2/3}$ for PEA_2SnI_4. The average power law scaling between broadening features and field is 0.39. **(F)** Peak amplitudes as a function of F^2 for PEA_2SnI_4. The peak E is influenced by a Stark shift of the above gap absorption peak γ and therefore does not exhibit the subquadric of 'E' in its lead counterpart.

Further evidence of the low-field to high-field transition within our experimental fields strengths lies in the amplitude scaling of EA features as a function of field strength. As shown in **Figure 6C**, peaks A, C, and E scale subquadratically with field for PEA_2PbI_4 (identical behavior is observed in BA_2PbI_4). The scaling decreases at higher energies with $k = 1.8$ for peak A, $k = 1.7$ for peak C, and $k = 1.4$ for peak E indicating these features have high-field FK character. As is clear from the trend of peak E in **Figure 6C**, k is not consistent across the entire field range, rather, it decreases as the high-field FK regime is

approached. Comparatively, the excitonic features retain F^2 dependence throughout the entire range of field strengths. Despite showing the most field-broadening, the PEA_2SnI_4 peaks do not decrease in amplitude as significantly: $k = 2.2$ for peak A, $k = 1.8$ for peak C, and $k = 2.2$ for peak E. The elevated k at peak E likely arises from spectral overlap of the neighboring γ peak at 2.12 eV. It is clear in the tin-based 2D MHPs that these above gap peaks experience Stark shifts as evidenced by abrupt changes in above-gap EA signals (located at 2.12 and 2.28 eV for PEA_2SnI_4). Therefore, the above-gap oscillations in PEA_2SnI_4 and BA_2SnI_4 EA signal should be viewed a competitive overlap of low-field FK features and Stark shifts of the γ and δ peaks; no feature can be analyzed as a pure representation of the field effects on a single transition. Unfortunately, BA_2SnI_4 thin films were too conductive without an SnF_2 additive and FK features were not resolved. The presence of fluoride centers throughout the crystal structure likely destroys the coherence of continuum states required for the high-field FK effect. Nevertheless, in all 2D MHPs of pure A_2BX_4 compositions, the onset of high-field FK character is observed in the EA signals.

Tentative Conclusions and Future Work

The in-plane 2D MHP EA spectra are dominated by linear and quadratic Stark shifts of excitonic states. Near the band edge, the predominantly Stark shifted features spectrally overlap with FK oscillations and acquire 'high-field FK character', as evidenced by their field-dependent behavior, e.g. broadening and subquadratic amplitude scaling. The onset of such field dependence is much closer to the exciton for PEA_2SnI_4 as compared to PEA_2PbI_4, suggesting that the Sn → Pb substitution significantly reduces E_B in MHPs. We find that E_B in tin-based 2D MHPs cannot be measured via EA alone, and therefore we hope to supplement these findings with temperature-dependent PL, low-temperature reflectance, and/or magnetoabsorption in order to precisely measure the effect of the Sn → Pb substitution on E_B in MHPs. Finally, we report an anomalous trend observed robustly in all 2D MHPs, that is, the 2nd derivative component of the exciton's EA line shape significantly diminishes with temperature. We attribute this to the exciton's temperature dependent transition dipole moment which may arise from dynamic disorder. This should be investigated further by computationally simulating disorder-induced dipole moments in MHPs and experimentally measuring μ_{ge} and α_{ge} across a wide temperature range from temperature-dependent EA.

References

1.   Mitzi, D. B., Synthesis, Crystal Structure, and Optical and Thermal Properties of (C4H9NH3)2MI4 (M = Ge, Sn, Pb). *Chemistry of Materials* **1996,** *8* (3), 791-800.

2.   Mitzi, D. B.; Feild, C.; Harrison, W.; Guloy, A., Conducting tin halides with a layered organic-based perovskite structure. *Nature* **1994,** *369* (6480), 467-469.

3.   Ishihara, T.; Takahashi, J.; Goto, T., Optical properties due to electronic transitions in two-dimensional semiconductors. *Physical Review B* **1990,** *42* (17), 11099-11107.

4.   Kim, J. Y.; Lee, J.-W.; Jung, H. S.; Shin, H.; Park, N.-G., High-Efficiency Perovskite Solar Cells. *Chemical Reviews* **2020,** *120* (15), 7867-7918.

5.   Cao, Y.; Fatemi, V.; Fang, S.; Watanabe, K.; Taniguchi, T.; Kaxiras, E.; Jarillo-Herrero, P., Unconventional superconductivity in magic-angle graphene superlattices. *Nature* **2018,** *556* (7699), 43-50.

6.   Bai, Y.; Zhou, L.; Wang, J.; Wu, W.; McGilly, L. J.; Halbertal, D.; Lo, C. F. B.; Liu, F.; Ardelean, J.; Rivera, P.; Finney, N. R.; Yang, X.-C.; Basov, D. N.; Yao, W.; Xu, X.; Hone, J.; Pasupathy, A. N.; Zhu, X. Y., Excitons in strain-induced one-dimensional moiré potentials at transition metal dichalcogenide heterojunctions. *Nature Materials* **2020,** *19* (10), 1068-1073.

7.   Yuan, M.; Quan, L. N.; Comin, R.; Walters, G.; Sabatini, R.; Voznyy, O.; Hoogland, S.; Zhao, Y.; Beauregard, E. M.; Kanjanaboos, P.; Lu, Z.; Kim, D. H.; Sargent, E. H., Perovskite energy funnels for efficient light-emitting diodes. *Nature Nanotechnology* **2016,** *11* (10), 872-877.

8.   Chen, P.; Bai, Y.; Wang, S.; Lyu, M.; Yun, J. H.; Wang, L., In situ growth of 2D perovskite capping layer for stable and efficient perovskite solar cells. *Advanced Functional Materials* **2018,** *28* (17), 1706923.

9.   Dong, H.; Zhang, C.; Liu, X.; Yao, J.; Zhao, Y. S., Materials chemistry and engineering in metal halide perovskite lasers. *Chemical Society Reviews* **2020,** *49* (3), 951-982.

10.   Walters, G.; Wei, M.; Voznyy, O.; Quintero-Bermudez, R.; Kiani, A.; Smilgies, D. M.; Munir, R.; Amassian, A.; Hoogland, S.; Sargent, E., The quantum-confined Stark effect in layered hybrid perovskites mediated by orientational polarizability of confined dipoles. *Nature Communications* **2018,** *9* (1), 4214.

11.   Qian, L.; Sun, Y.; Sun, M.; Fang, Z.; Li, L.; Xie, D.; Li, C.; Ding, L., 2D perovskite microsheets for high-performance photodetectors. *Journal of Materials Chemistry C* **2019,** *7* (18), 5353-5358.

12.   Mao, L.; Stoumpos, C. C.; Kanatzidis, M. G., Two-dimensional hybrid halide perovskites: principles and promises. *Journal of the American Chemical Society* **2018,** *141* (3), 1171-1190.

13.   Straus, D. B.; Kagan, C. R., Electrons, excitons, and phonons in two-dimensional hybrid perovskites: connecting structural, optical, and electronic properties. *The journal of physical chemistry letters* **2018,** *9* (6), 1434-1447.

14.   Mauck, C. M.; Tisdale, W. A., Excitons in 2D organic–inorganic halide perovskites. *Trends in Chemistry* **2019,** *1* (4), 380-393.

15.   Baranowski, M.; Plochocka, P., Excitons in metal-halide perovskites. *Advanced Energy Materials* **2020,** *10* (26), 1903659.

16.   Neutzner, S.; Thouin, F.; Cortecchia, D.; Petrozza, A.; Silva, C.; Srimath Kandada, A. R., Exciton-polaron spectral structures in two-dimensional hybrid lead-halide perovskites. *Physical Review Materials* **2018,** *2* (6), 064605.

17.   Thouin, F.; Valverde-Chávez, D. A.; Quarti, C.; Cortecchia, D.; Bargigia, I.; Beljonne, D.; Petrozza, A.; Silva, C.; Srimath Kandada, A. R., Phonon coherences reveal the polaronic character of excitons in two-dimensional lead halide perovskites. *Nature Materials* **2019,** *18* (4), 349-356.

18.   Blancon, J. C.; Stier, A. V.; Tsai, H.; Nie, W.; Stoumpos, C. C.; Traoré, B.; Pedesseau, L.; Kepenekian, M.; Katsutani, F.; Noe, G. T.; Kono, J.; Tretiak, S.; Crooker, S. A.; Katan, C.; Kanatzidis, M. G.; Crochet, J. J.; Even, J.; Mohite, A. D., Scaling law for excitons in 2D perovskite quantum wells. *Nature Communications* **2018,** *9* (1), 2254.

19.   Tanaka, K.; Takahashi, T.; Kondo, T.; Umebayashi, T.; Asai, K.; Ema, K., Image charge effect on two-dimensional excitons in an inorganic-organic quantum-well crystal. *Physical Review B* **2005,** *71* (4), 045312.

20.   Amerling, E.; Baniya, S.; Lafalce, E.; Zhang, C.; Vardeny, Z. V.; Whittaker-Brooks, L., Electroabsorption Spectroscopy Studies of (C4H9NH3)2PbI4 Organic–Inorganic Hybrid Perovskite Multiple Quantum Wells. *The Journal of Physical Chemistry Letters* **2017,** *8* (18), 4557-4564.

21.   Zhai, Y.; Baniya, S.; Zhang, C.; Li, J.; Haney, P.; Sheng, C.-X.; Ehrenfreund, E.; Vardeny, Z. V., Giant Rashba splitting in 2D organic-inorganic halide perovskites measured by transient spectroscopies. *Science Advances* **2017,** *3* (7), e1700704.

22.   Miller, D. A. B.; Chemla, D. S.; Damen, T. C.; Gossard, A. C.; Wiegmann, W.; Wood, T. H.; Burrus, C. A., Band-Edge Electroabsorption in Quantum Well Structures: The Quantum-Confined Stark Effect. *Physical Review Letters* **1984,** *53* (22), 2173-2176.

23.   Miller, D. A. B.; Chemla, D. S.; Damen, T. C.; Gossard, A. C.; Wiegmann, W.; Wood, T. H.; Burrus, C. A., Electric field dependence of optical absorption near the band gap of quantum-well structures. *Physical Review B* **1985,** *32* (2), 1043-1060.

24.   Tanaka, K.; Takahashi, T.; Kondo, T.; Umeda, K.; Ema, K.; Umebayashi, T.; Asai, K.; Uchida, K.; Miura, N., Electronic and Excitonic Structures of Inorganic–Organic Perovskite-Type Quantum-Well Crystal (C4H9NH3)2PbBr4. *Japanese Journal of Applied Physics* **2005,** *44* (8), 5923-5932.

25.   Tanaka, K.; Sano, F.; Takahashi, T.; Kondo, T.; Ito, R.; Ema, K., Two-dimensional Wannier excitons in a layered-perovskite-type crystal (C6H13NH3)2PbI4. *Solid State Communications* **2002,** *122* (5), 249-252.

26.   Kneissl, M.; Linder, N.; Kiesel, P.; Quassowski, S.; Schmidt, K.; Döhler, G. H.; Grothe, H.; Smith, J. S., Two-dimensional Franz-Keldysh effect in MQW structures with lateral electric fields. *Superlattices and Microstructures* **1994,** *16* (2), 109.

27.   Kattoor, V.; Awasthi, K.; Jokar, E.; Diau, E. W.-G.; Ohta, N., Integral Method Analysis of Electroabsorption Spectra and Electrophotoluminescence Study of (C4H9NH3)2PbI4 Organic–Inorganic Quantum Well. *The Journal of Physical Chemistry C* **2018,** *122* (46), 26623-26634.

28.   Zhang, F.; Zhang, H.; Zhu, L.; Qin, L.; Wang, Y.; Hu, Y.; Lou, Z.; Hou, Y.; Teng, F., Two-dimensional organic–inorganic hybrid perovskite field-effect transistors with polymers as bottom-gate dielectrics. *Journal of Materials Chemistry C* **2019,** *7* (14), 4004-4012.

29.   Chen, C.; Zhang, X.; Wu, G.; Li, H.; Chen, H.; Zhang, X., Visible-Light Ultrasensitive Solution-Prepared Layered Organic-Inorganic Hybrid Perovskite Field-Effect Transistor. *Adv. Opt. Mater. Advanced Optical Materials* **2017,** *5* (2).

30.   Febriansyah, B.; Lim, M. H.; England, J.; Febriansyah, B.; Harikesh, P. C.; Koh, T. M.; Shen, Z. X.; Mathews, N.; Febriansyah, B.; Harikesh, P. C.; Lekina, Y.; Shen, Z. X.;

Kaur, J.; Chakraborty, S.; Hooper, T. J. N.; Mathews, N., Formation of Corrugated 2D Tin Iodide Perovskites and Their Use as Lead-Free Solar Absorbers. *ChemRxiv ChemRxiv* **2020**.

31.   Dong, J.; Shao, S.; Kahmann, S.; Rommens, A. J.; Hermida-Merino, D.; ten Brink, G. H.; Loi, M. A.; Portale, G., Mechanism of Crystal Formation in Ruddlesden-Popper Sn-Based Perovskites. *Advanced Functional Materials* **2020,** *30* (24).

32.   Weiser, G., Stark effect of one-dimensional Wannier excitons in polydiacetylene single crystals. *Physical Review B* **1992,** *45* (24), 14076-14085.

33.   Lanzani, G., The photophysics behind photovoltaics and photonics. **2012**.

34.   Liptay, W., Optical Absorption of Molecules in Liquid Solutions in an Applied External Electric Field (Electrochromism). *BBPC Berichte der Bunsengesellschaft f,r physikalische Chemie* **1976,** *80* (3), 207-217.

35.   Horvath, A.; Weiser, G.; Baker, G. L.; Etemad, S., Influence of disorder on the field-modulated spectra of polydiacetylene films. *Physical Review B* **1995,** *51* (5), 2751-2758.

36.   Dow, J. D.; Redfield, D., Electroabsorption in Semiconductors: The Excitonic Absorption Edge. *Physical Review B* **1970,** *1* (8), 3358-3371.

37.   Lederman, F. L.; Dow, J. D., Theory of electroabsorption by anisotropic and layered semiconductors. I. Two-dimensional excitons in a uniform electric field. *Physical Review B* **1976,** *13* (4), 1633-1642.

38.   Ziffer, M. E.; Mohammed, J. C.; Ginger, D. S., Electroabsorption Spectroscopy Measurements of the Exciton Binding Energy, Electron–Hole Reduced Effective Mass, and Band Gap in the Perovskite CH3NH3PbI3. *ACS Photonics* **2016,** *3* (6), 1060-1068.

39.   Aspnes, D. E., Electric-Field Effects on Optical Absorption near Thresholds in Solids. *Physical Review* **1966,** *147* (2), 554-566.

40.   Jaeger, A.; Weiser, G.; Wiedemann, P.; Gyuro, I.; Zielinski, E., The sizes of coherent band states in semiconductors, derived from the Franz - Keldysh effect. *Journal of Physics: Condensed Matter* **1996,** *8* (36), 6779-6789.

41.   Shen, H.; Dutta, M., FranzKeldysh oscillations in modulation spectroscopy. *Journal of Applied Physics Journal of Applied Physics* **1995,** *78* (4), 2151-2176.

42.   Hamakawa, Y.; Germano, F. A.; Handler, P., Interband Electro-Optical Properties of Germanium. I. Electroabsorption. *Physical Review* **1968,** *167* (3), 703-709.

43.   Aspnes, D. E.; Rowe, J. E., Resonant Nonlinear Optical Susceptibility: Electroreflectance in the Low-Field Limit. *Physical Review B* **1972,** *5* (10), 4022-4030.

44.   Byrnes, S. J., Multilayer optical calculations. *arXiv preprint arXiv:1603.02720* **2016**.

45.   Proppe, A. H.; Walters, G. W.; Alsalloum, A. Y.; Zhumekenov, A. A.; Mosconi, E.; Kelley, S. O.; De Angelis, F.; Adamska, L.; Umari, P.; Bakr, O. M.; Sargent, E. H., Transition Dipole Moments of n = 1, 2, and 3 Perovskite Quantum Wells from the Optical Stark Effect and Many-Body Perturbation Theory. *The Journal of Physical Chemistry Letters* **2020,** *11* (3), 716-723.

46.   Tai, K.; Hegarty, J.; Tsang, W. T., Observation of optical Stark effect in InGaAs/InP multiple quantum wells. *Appl. Phys. Lett. Applied Physics Letters* **1987,** *51* (3), 152-154.

47.   Von Lehmen, A.; Chemla, D. S.; Zucker, J. E.; Heritage, J. P., Optical Stark effect on excitons in GaAs quantum wells. *Opt. Lett.* **1986,** *11* (10), 609-11.

48.   Weiser, G., Absorption and electroabsorption on amorphous films of polyvinylcarbazole and trinitrofluorenone. *PSSA physica status solidi (a)* **1973,** *18* (1), 347-359.

49.   Labhart, H., Bestimmung von moleküleigenschaften aus elektrooptischen effekten. *TET Tetrahedron: Supplement 2* **1963,** *19*, 223-241.

50.   Liptay, W.; Eberlein, W.; Weidenberg, H.; Elflein, O., Die Beeinflussung der optischen Absorption von Molekülen durch ein äußeres elektrisches Feld. V. Übergangsmomentrichtungen und Dipolmomente der niedrigen Elektronenzustände in 4-Nitranilin, 1-Nitro-3,5-diaminobenzol, 3,5-Dinitroanilin, Carbazol und 3,6-Dinitrocarbazol. *BBPC Berichte der Bunsengesellschaft für physikalische Chemie* **1967,** *71* (6), 548-560.

51.   Leguy, A. M. A.; Goñi, A. R.; Frost, J. M.; Skelton, J.; Brivio, F.; Rodríguez-Martínez, X.; Weber, O. J.; Pallipurath, A.; Alonso, M. I.; Campoy-Quiles, M.; Weller, M. T.; Nelson, J.; Walsh, A.; Barnes, P. R. F., Dynamic disorder, phonon lifetimes, and the assignment of modes to the vibrational spectra of methylammonium lead halide perovskites. *Physical Chemistry Chemical Physics* **2016,** *18* (39), 27051-27066.

52.   Kang, J.; Wang, L.-W., Dynamic Disorder and Potential Fluctuation in Two-Dimensional Perovskite. *The Journal of Physical Chemistry Letters* **2017,** *8* (16), 3875-3880.

53.   Chen, Z.; Zhu, M.; Loh, K. P.; Xu, Q. H.; Zhang, Q.; Wang, X.; Wang, Q.; Wee, A. T. S.; Eda, G.; Zhu, M.; Wee, A. T. S.; Loh, K. P.; Xu, Q. H., Synthesis of Two-Dimensional Perovskite by Inverse Temperature Crystallization and Studies of Exciton States by Two-Photon Excitation Spectroscopy. *Adv. Funct. Mater. Advanced Functional Materials* **2020,** *30* (31).

54.   Horvath, A.; Kolbe, H. J.; Weiser, G.; Optics; Photonics; Optical Science, E.; Instrumentation; San Diego, C. A. U. S.; Optical Probes of Conjugated, P.; Photoexcitations, I. I. S., Franz-Keldysh effect of band states in polydiacetylene. **1997,** *3145*, 152-162.

55.   Sebastian, L.; Weiser, G., One-dimensional wide energy bands in a polydiacetylene revealed by electroreflectance. *Physical Review Letters* **1981,** *46* (17), 1156.